Deep-learning-empowered synthetic dimension dynamics: morphing of light into topological modes

Xia, Shiqi; Lei, Sihong; Song, Daohong; Di Lauro, Luigi; Alamgir, Imtiaz; Tang, Liqin; Xu, Jingjun; Morandotti, Roberto; Buljan, Hrvoje; Chen, Zhigang

Research Article

ADVANCED PHOTONICS

Deep-learning-empowered synthetic dimension dynamics: morphing of light into topological modes

Shiqi Xia,[a,†] Sihong Lei,[a,†] Daohong Song,[a,b] Luigi Di Lauro,[c] Imtiaz Alamgir,[c] Liqin Tang,[a,b] Jingjun Xu,[a] Roberto Morandotti,[c] Hrvoje Buljan,[a,d,*] and Zhigang Chen[a,b,*]

[a]Nankai University, TEDA Institute of Applied Physics, School of Physics, The MOE Key Laboratory of Weak-Light Nonlinear Photonics, Tianjin, China
[b]Shanxi University, Collaborative Innovation Center of Extreme Optics, Taiyuan, China
[c]INRS-EMT, Varennes, Quebec, Canada
[d]University of Zagreb, Department of Physics, Faculty of Science, Zagreb, Croatia

Abstract. Synthetic dimensions (SDs) opened the door for exploring previously inaccessible phenomena in high-dimensional space. However, construction of synthetic lattices with desired coupling properties is a challenging and unintuitive task. Here, we use deep learning artificial neural networks (ANNs) to construct lattices in real space with a predesigned spectrum of mode eigenvalues, and thus to validly design the dynamics in synthetic mode dimensions. By employing judiciously chosen perturbations (wiggling of waveguides at desired frequencies), we show resonant mode coupling and tailored dynamics in SDs. Two distinct examples are illustrated: one features uniform synthetic mode coupling, and the other showcases the edge defects that allow for tailored light transport and confinement. Furthermore, we demonstrate morphing of light into a topologically protected edge mode with modified Su–Schrieffer–Heeger photonic lattices. Such an ANN-assisted construction of SDs may advance toward "utopian networks," opening new avenues for fundamental research beyond geometric limitations as well as for applications in mode lasing, optical switching, and communication technologies.

Keywords: synthetic dimensions; deep learning; mode manipulation; topological mode morphing; photonic lattices.

Received Oct. 1, 2023; revised manuscript received Jan. 26, 2024; accepted for publication Feb. 20, 2024; published online Mar. 18, 2024.

[DOI: 10.1117/1.AP.6.2.026005]

1 Introduction

Synthetic dimensions (SDs) are drawing a great deal of interest in topological photonics and other branches of physics for exploiting fundamental phenomena in high-dimensional spaces.[1,2] Several theoretical proposals have been put forward for the study and implementation of synthetic gauge fields, quantum Hall physics, discrete solitons, Weyl semimetals, and topological phase transitions in four dimensions and beyond, predicting rich physics inaccessible in a conventional three-dimensional real space.[3–8] In particular, it is quite challenging to realize experimentally a complex lattice structure or network of resonators with anisotropic, long-range or dissipative couplings in real space, but that is particularly amenable using SDs. Examples include demonstrations of non-Hermitian topological winding,[9,10] skin effect,[11] parity-time symmetry,[12,13] topological "triple" phase transition,[14] and nontrivial topology arising from a system's dissipation.[15] Thus far, SDs have been constructed using a variety of parameters or degrees of freedom in a given system, such as frequency modes, spatial modes, orbital angular momenta, and time-delayed pulses,[11,14–22] along with many proposed applications in, for example, optical communications and topological insulator lasers.[23,24]

One highly desirable goal of these studies is to construct a "utopian" network of resonators or coupled modes, where any pair of modes could be coupled in a controlled fashion.[25]

*Address all correspondence to Hrvoje Buljan, hbuljan.phy@pmf.hr; Zhigang Chen, zgchen@nankai.edu.cn

†These authors contributed equally to this work.

However, in most systems, the possibilities depend on their natural properties. For example, the realization of resonant coupling strongly depends on a given spectrum of eigenvalues. Moreover, mode manipulation has emerged as an active research subject in many photonic systems,[26] as it brings about new possibilities for improving the design and functionality of devices. For instance, appropriate mode manipulation can increase the capacities of data transmission,[27,28] enhance the efficiency of energy harvesting,[11] and enlarge the radiance of laser arrays.[29] Recently, mode manipulation using the concepts of non-Hermiticity, nonlinear topological photonics, as well as optical thermalization has been proposed and demonstrated,[30,31] which rely in large part on the gain-loss feature, nonreciprocal couplings, and light–matter interactions.

In this work, we implement on-demand waveguide arrays with desired features in SDs, so as to achieve tailored mode manipulation in a linear system without the need to introduce non-Hermiticity or nonlinearity. Such manipulation of the modal spectrum brings us one step further toward the utopian networks.[25] The mode manipulation is achieved by introducing perturbations with a particular frequency (or frequencies) that corresponds to the spacing between mode eigenvalues. We use pre-trained artificial neural networks (ANNs) to design a waveguide array (i.e., a photonic lattice) in real space, which has a predetermined spectrum of eigenvalues (see Fig. 1). We experimentally implement two mode arrays in SDs: one with uniform synthetic mode coupling strengths, and the other with edge defect weakly coupled to the bulk in the SD, showing correspondingly light transport and confinement in the SD. Finally, we utilize ANNs to design a modified type of Su–Schrieffer–Heeger (SSH) topological lattice[32] that has a linear dispersion in bulk bands, and thereby to demonstrate controlled coupling in the SD and morphing of light from a given bulk mode into a topological edge state.

2 Principles and Methods

2.1 Deep-Learning-Empowered Eigenvalue Design

The eigenmodes and eigenvalues of any Hamiltonian H can in principle be found by diagonalization, which produces a transformation matrix Φ comprising eigenmodes of H. The diagonal matrix $E = \Phi^{\dagger} H \Phi$ contains the eigenvalues, conveniently written as an array $B = \mathrm{diag}(E)$. Previous analytical methods, such as the Lanczos method and Householder transformations, have offered approaches to solve or modify the spectrum based on a Hamiltonian provided beforehand.[29,33] However, the inverse problem is far more complicated: given a preassigned eigenvalue

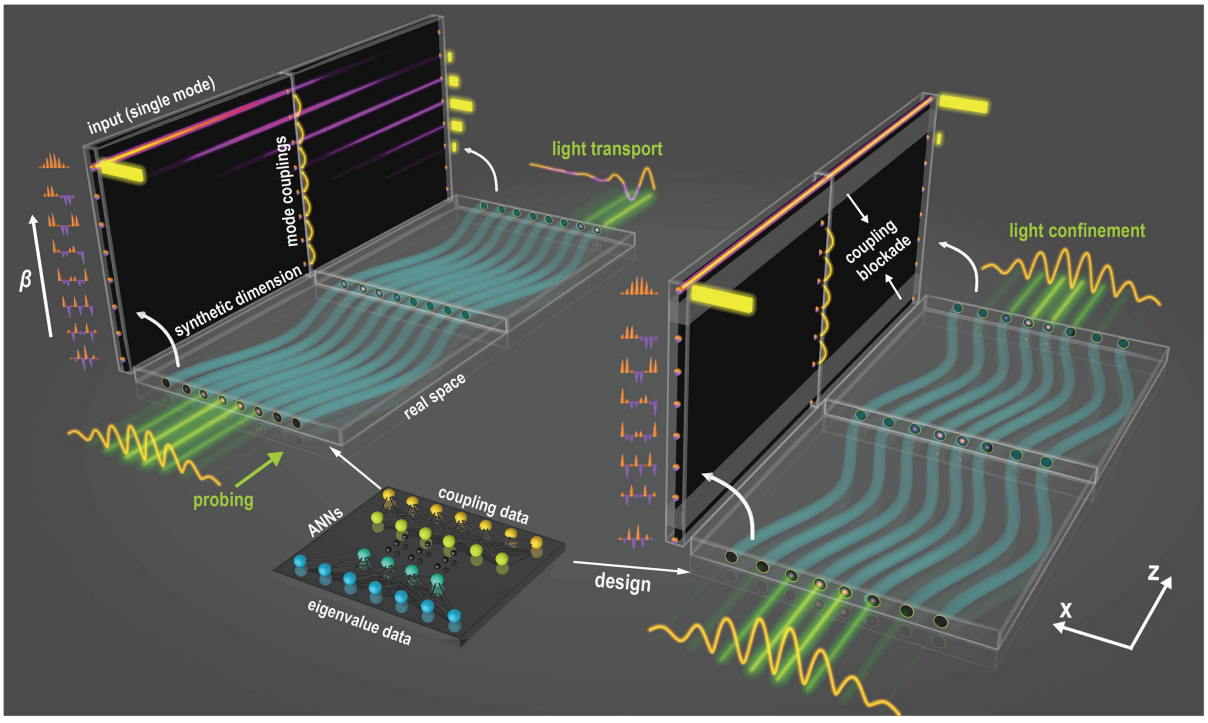

Fig. 1 Scheme for the mode manipulation in SD assisted with ANNs. A probe beam at input representing one mode (edge in SD) is launched into different synthetic mode arrays, through which light is either transported laterally (left) or confined in SD but as a complex profile in real space (right), depending on the ANN design of the arrays. The input and output data of the ANNs are based on the preassigned eigenvalues and couplings of the arrays. Waveguides are curved along the z direction in real space. Vertical planes show the mode evolution in SD, where orange/purple profiles lined up vertically are the eigenmode distributions, forming the lattices in SD. The yellow bars denote the mode distribution of the probe beam, and the shaded zone (in right panel) represents a coupling blockade in SD. The curved lines depicted at the input and output facets of the arrays represent the complex beam profile in real space, which is well maintained during propagation in the right panel due to the proper design of the coupling blockade.

array $B = \mathrm{diag}(E)$, what is the Hamiltonian H with such eigenvalues? Moreover, this task is here constrained with physical implementation: we demand that only the coupling between the nearest neighbor waveguides is present in the Hamiltonian, which is consistent with experimental conditions employing evanescently coupled waveguides. In this work, we employ deep learning[34,35] to find the Hamiltonian that yields a desired eigenvalue array B.

The deep-learning method, a subset of machine learning that uses ANNs, has been applied in many physical systems, including photonics, image recognition, data analysis, and inverse design.[36–39] This is in contrast to previous work of all-optically implemented ANNs, in which researchers explored the realm of all-optical computation,[40,41] and the algorithm was utilized to address the inverse design problem.[38] A general description of the ANN paradigm we used can be found in the Supplementary Material. Here, we use a preassigned eigenvalue array B as the input layer data of the ANNs [Fig. 2(a1)]. The number of modes is chosen to be $N = 8$, but our method can be readily applied for larger systems (see the Supplementary Material). The couplings between nearest neighbor sites, which define the Hamiltonian H, are assigned as the output layer. To determine the values of weights in all hidden layers, 800 sets of eigenvalue-Hamiltonian data (obtained numerically with the tight-binding model) are sent to the ANNs to train the networks (see the Supplementary Material).

When the ANN training is completed, two preassigned eigenvalue arrays B illustrated in Figs. 2(a1) and 2(b1) are sent back to the ANNs. The first array [Fig. 2(a1)] is an equally spaced array, whereas the second one [Fig. 2(b1)] has two outlying eigenvalues at the edges of the SD.[42] For each of the eigenvalue arrays, the ANNs [Fig. 2(a1)] yield a corresponding tight-binding Hamiltonian of the form

$$H_A = \sum_{n=1}^{N-1} t_n c_{n+1}^{\dagger} c_n + \mathrm{H.c.}, \tag{1}$$

where $c_n^{\dagger}$ and c_n are the creation and annihilation operators on the nth site in real space, t_n is the coupling coefficient between the nth and $(n+1)$th sites, and H.c. stands for the Hermitian conjugation. The eigenvalues of H_A are given by $E_A = \Phi_A^{\dagger} H_A \Phi_A$. To evaluate the effectiveness of our ANN method, we use the following figure of merit:

$$\gamma_B = \frac{1}{N} \sum_{m=1}^{N-1} |\Delta\beta_{Am} - \Delta\beta_m| / \Delta\beta_m, \tag{2}$$

where β_m is the propagation constant of the mth mode, and $\Delta\beta_m$ ($\Delta\beta_{Am}$) is the eigenvalue difference between the mth and $(m+1)$th mode in the preassigned (ANN-calculated) eigenvalue array. The figure of merit compares the difference between the eigenvalues because it determines the coupling of modes in SD driven by perturbations. We find that γ_B is ~0.90% for the mode array with equal spacing, and $\gamma_B = 3.15\%$ for the array with outlying edges. The low deviations calculated for these two different mode arrays show the high effectiveness of our ANN method.

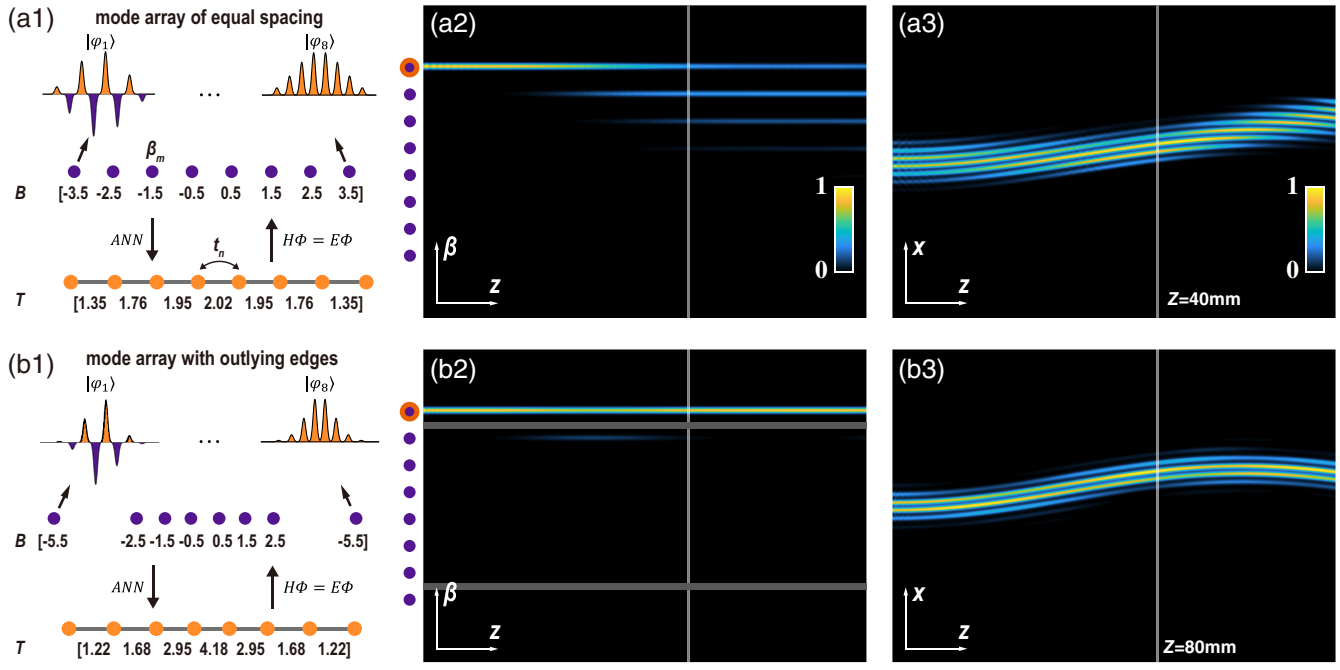

Fig. 2 Illustration of the mode evolution in different mode arrays designed by ANNs. (a1)–(a4) Illustration of the mode arrays with equal spacing of eigenvalues β_m. (a1) The sketch of the eigenvalue array B and corresponding eigenmodes $|\varphi_i\rangle$. The arrangement of the coupling array in real space (labeled T) is calculated by ANNs. (a2) The mode evolution dynamics in SD. Orange circle in the left column indicates the excited mode. (a3) The corresponding beam propagation dynamics in real space. (b1)–(b3) have the same layout as (a1)–(a3), except that they are for the mode arrays with outlying edges, showing that the excited mode is well confined in SD. The shaded zones in (b2) show the coupling blockades between the edge and bulk modes in SD. The propagation distances at the vertical lines in (a) and (b) are for $Z = 40$ mm and $Z = 80$ mm, respectively.

2.2 Construction of Synthetic Mode Dimension

By appropriately wiggling the waveguides along the propagation direction (Fig. 1), we engineer the coupling between eigenmodes of the Hamiltonian H_A; that is, we engineer the dynamics in SD[20] (see the Supplementary Material). Let D_n denote the equilibrium distance between the first and nth waveguides. If the center of each waveguide wiggles along the propagation direction as $R\ \sin(\Omega z+\theta)$ in the (x,z) plane, in analogy with quantum mechanics, it is equivalent to introducing an oscillating scalar potential $V(x,z)=V_0\ \sin(\Omega z+\theta)(x-D_N/2)$. Here, we have for convenience set the zero point of the potential $V(D_N/2)=0$ to be the central point of our lattice denoted with $D_N/2$, where the D_N is the distance between the first and last (Nth) waveguides. The amplitude $V_0=k_0\Omega^2R$ can be calculated for our system straightforwardly in a vector potential gauge[20] (see the Supplementary Material); here $k_0=2\pi n_0/\lambda$ is the wavenumber (n_0 is the refractive index of the medium, and λ is the wavelength). After applying the wiggling, the discrete Hamiltonian becomes

$$H_w(z)=H_A+H_1(z),$$
$$H_1(z)=\sum_{n=1}^{N}(D_n-D_N/2)k_0\Omega^2R\ \sin(\Omega z+\theta)c_n^{\dagger}c_n+\text{H.c.}\quad(3)$$

Here, z indicates the propagation distance along the photonic lattices, which is equivalent to the role of time in quantum mechanics. The scalar potential $V(x,z)$ is applied to the onsite terms. It is important to acknowledge that the mode coupling in SDs is not an adiabatic process, as in Thouless pumping.[43,44] In the language of quantum mechanics, we utilize appropriately tailored time-dependent perturbations to transfer the energy between eigenmodes in a controllable fashion, which is enabled by the preassigned energies that enter the ANNs. The on-site terms in the SD Hamiltonian are given by the diagonal matrix $\Phi_A^{\dagger}H_A\Phi_A$, and the wiggling-induced coupling coefficients are contained in the matrix $\Phi_A^{\dagger}H_1(z)\Phi_A$[20] (see the Supplementary Material); note that the oscillating term $\sin(\Omega z+\theta)$ can be extracted from the latter expression. It is worth mentioning that the matrix elements (i.e., the strength of the coupling) depend on the mode structure, which cannot be fully controlled by the current method. Nevertheless, in our cases, we can get the matrix elements after the transformation, as shown and discussed in the Note 2 in the Supplementary Material.

2.3 Mode Evolution in Different Synthetic Mode Arrays

For the mode array with equal spacing between the propagation constants, the two nonzero off-diagonals indicate dominance of the nearest neighbor coupling in SD (see the Supplementary Material). The wiggling frequency is identical to the equal spacing between the propagation constants (we use a dimensionless tight-binding model here). By using the proper rotating-wave approximation, which is here equivalent to interaction picture in quantum mechanics, the linear on-site potential in $\Phi_A^{\dagger}H_0\Phi_A$ is eliminated (see the Supplementary Material), where H_0 has the same mathematical expression as H_A; see more details in the Supplementary Material.[20] Therefore, the structure in Fig. 2(a) can be regarded as a one-dimensional (1D) waveguide array in SD. If the mode circled in Fig. 2(a2) is initially excited, it undergoes discrete diffraction in SD, shown in the numerical simulation.

For the mode array with outlying edges sketched in Fig. 2(b), in the interaction picture, the on-site energies of the bulk modes in SD are zero, but the on-site energies of the outlying modes differ; see more details in the Supplementary Material. The modes inside the coupling blockades are mutually well coupled with nearest neighbor interactions [Fig. 2(b2)]. However, the two outlying modes are only weakly coupled to the bulk. This is the consequence of the ANN-engineered spectra of the propagation constants. We find some minor long-range couplings between modes; however, the percentage of the maximum of long-range couplings over the minimum nearest neighbor couplings is ~8.64%; thus, they can be ignored. The mode transport and confinement in SD are further simulated using the continuous model (see the Supplementary Material).

3 Results

3.1 CW-Laser-Writing Technique and Cascade-Probing Method

To experimentally demonstrate the aforementioned system design in SD, we apply the cw-laser-writing technique (with a wavelength of 532 nm and a power of 100 mW for the writing beam, as well as an applied field of 200 kV/m in the biased crystal) developed earlier for inducing photonic lattices laterally from the top of a strontium barium niobate (SBN:61) nonlinear crystal.[45] The wiggling frequency and amplitude of the writing beam are tuned by a spatial light modulator (SLM). To clearly see the difference of mode evolution in the two different mode arrays, a long propagation distance is needed. Due to the restriction of the crystal length ($L=20$ mm) in the experiment, the whole waveguide array is divided into several sections along the propagation direction. Each section is laterally written into the crystal in sequence, thus effectively lengthening the propagation distance [Fig. 3(a)]. Meanwhile, we develop a cascade-probing method to illustrate the mode coupling in SD. The amplitude and phase of the output beam (with a wavelength of 532 nm and a power of 2 μW) from one waveguide section are recorded by a camera,[46] digitally duplicated by the SLM, and then launched into the next section of the waveguide arrays as an input [Fig. 3(a)]. Since the duplicated beam carries all the amplitude and phase information from one section to another, such cascade probing equivalently "glues" all parts of the waveguide arrays together, therefore allowing us to examine mode evolution through long arrays (see the Supplementary Material).

3.2 Observation of the Synthetic Dynamics in Different Mode Arrays

The coupling strength in SD is controlled by the distance between the nearest waveguides and a proper wiggling frequency of the writing beam $\Omega=58.70\ \text{m}^{-1}$, which is determined according to the corresponding simulation (see the Supplementary Material). The selected eigenmode of the lattice is generated by the SLM in the experiment and is used as the probe beam. With the cascade probing method, the output intensity and phase distributions of the probe beam at $z=20$ mm and 40 mm in real space are extracted and plotted in Figs. 3(b1) and 3(b2) together with results of numerical simulations from the continuous model (see the Supplementary Material). The deviation in the phase distributions at some sites has very minor effect on the

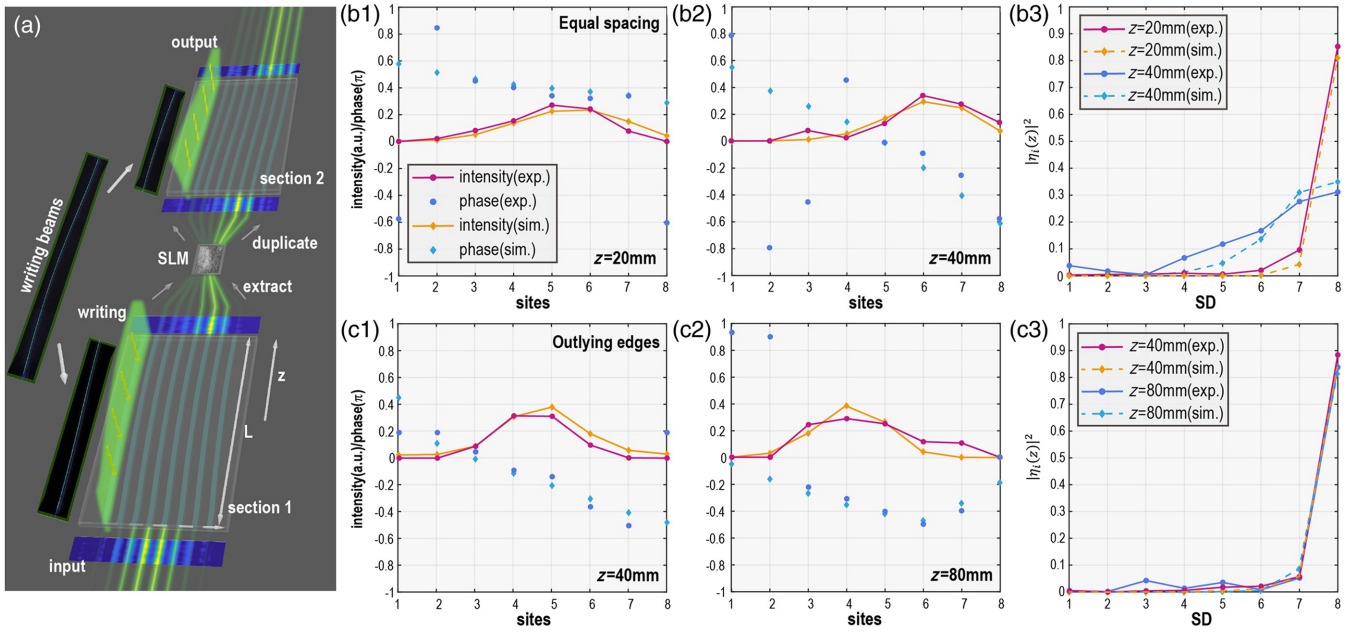

Fig. 3 Experimental demonstration of mode manipulation in SD and corresponding simulations. (a) Illustration of the cw-laser writing and cascade probing method in the experiment. Curved waveguide arrays are written section by section (from the top of a nonlinear crystal), and the output of the probe beam (propagating through the arrays along the z direction) from one section is taken as the input for the subsequent section assisted with the SLM, thus effectively increasing the propagation distance. (b) Results from the mode array with equal spacing, where (b1) and (b2) show the output amplitude and phase distribution from the experiment and simulation at $z = 20$ and 40 mm. (b3) The corresponding output distribution in SD. (c1)–(c3) Results from the mode array with outlying edges, with the same layout as (b1)–(b3) but at even longer propagation distances, showing confinement of the excited mode in both real space and SD.

output mode distributions, since the intensity at those sites is negligible. The complex amplitude of the output beam $\psi(z) = \sqrt{I(z)}\exp(i\alpha(z))$, where $I(z)$ and $\alpha(z)$ are the measured intensity and phase, is projected onto the eigenmodes,

$$\eta_i(z) = \langle \varphi_i | \psi(z) \rangle. \tag{4}$$

The overlap values $|\eta_i(z)|^2$ for every mode at $z = 20$ mm and 40 mm are plotted in Fig. 3(b3). The main components reside on the initially excited mode at $z = 20$ mm. However, at a longer propagation distance ($z = 40$ mm), the probe beam spreads into the neighboring modes [Fig. 3(b3)], in the mode array with equal spacing. The experimental results and simulations agree well.

On the other hand, in the mode array with outlying edges, the wiggling frequency of the waveguide is set to $\Omega = 30.55\ \mathrm{m}^{-1}$ (see the Supplementary Material). The total propagation length is set to $L = 40$ mm in the mode array of equal spacing and $L = 80$ mm in the mode array with outlying edges to roughly have the same ΩL as for the array with equal spacing. Under the same initial excitation, the intensity and phase distributions at $z = 40$ and 80 mm are plotted in Figs. 3(c1) and 3(c2), which again agree well with simulations. Most importantly, the dynamics in SD [Fig. 3(c3)] indicates the confinement of the initially excited mode in the mode array with outlying edges, which corresponds to the effective guidance of a complex beam profile observed in the experiment [Figs. 3(c1) and 3(c2)].

3.3 Morphing of Light into Topological Modes

To illustrate the power of our ANN-designed dynamics in SD, we modify the 1D SSH lattice by ANNs to obtain bands with linear dependence of energy on the mode number and use these structures to obtain morphing of the initially excited bulk mode into a topological edge mode residing in the gap (see Fig. 4). It is important to note that our intent is not just to construct an SSH model in the framework of SD[18] or real space,[47–49] but rather to utilize SD to realize nontrivial mode couplings. In Figs. 4(a1) and 4(b1), we plot the eigenvalues of a trivial and nontrivial SSH lattice, respectively, with $N = 12$ sites; note that the eigenvalue separations between the modes in the bands are identical, i.e., we have linear dependence of β_n on the mode number n (see the Supplementary Material). The nontrivial lattice [Fig. 4(b1)] in addition possesses two topological modes in the gap; they are topological because the conventional SSH lattice can be continuously deformed in our ANN-designed lattice without closing the gap, showing its robustness against disorders (see the Supplementary Material). First, we excite the mode in the trivial SSH lattice, which is adjacent to the gap [Fig. 4(a2)], and wiggle the lattice with frequency identical to the eigenvalue spacing between adjacent modes in the bands ($\Delta\beta = \Omega$). Due to the presence of the gap and the chosen wiggling frequency, the initially excited mode can couple only to the adjacent mode in its own band (it cannot cross the gap). Thus, dynamics in SD corresponds to discrete transport of light restricted to one band [Fig. 4(a2)]. The corresponding dynamics in real space is shown

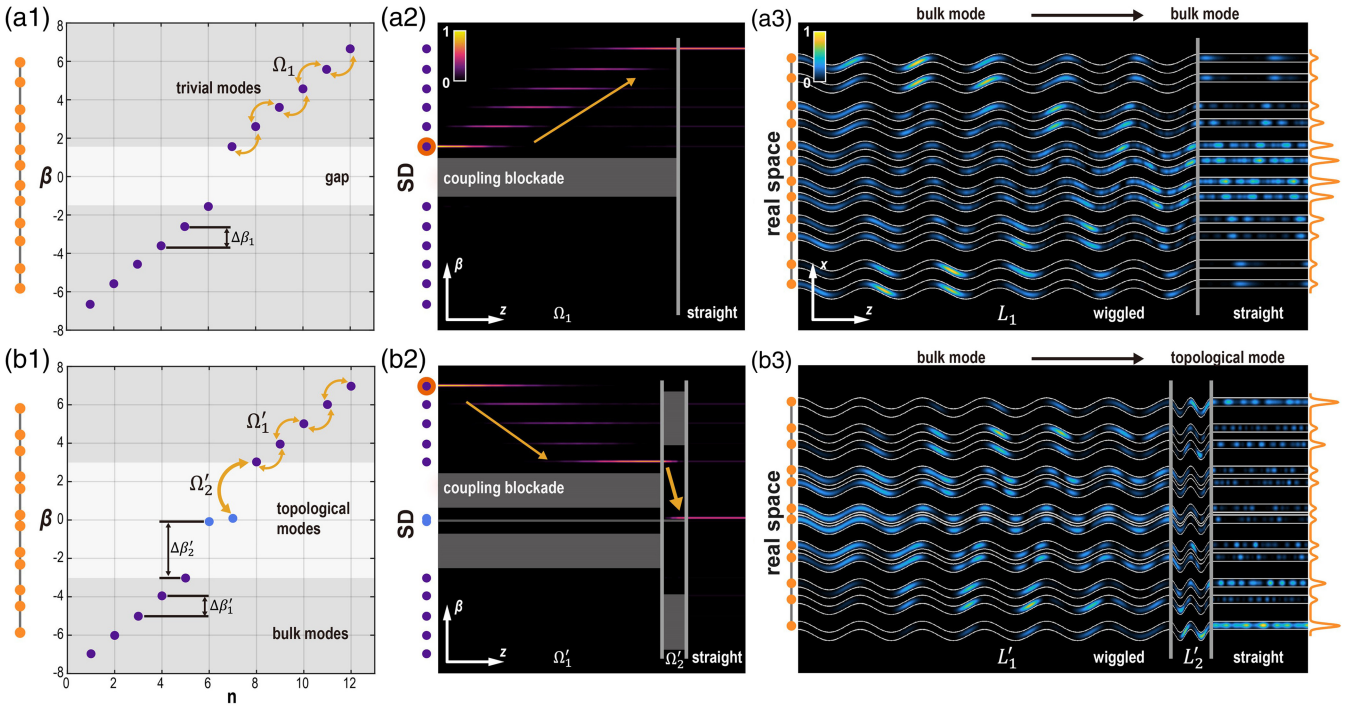

Fig. 4 Mode switching and morphing into topological modes by tuning the array in SD. (a) Mode switching between bulk modes in a topologically trivial lattice designed by ANNs. (a1) The lattice illustration in real space (far left column) and corresponding eigenvalue distribution (right panel). Bulk modes above or below the gap couple to each other without a coupling blockade under an array wiggling frequency $\Omega_1 = 1$ and the eigenvalue difference $\Delta\beta_1 = 1$. (a2) Mode evolution during propagation in SD, where the orange circle indicates the initially excited mode. The second region distinguished by the vertical lines is straight waveguides. The shaded zones indicate the coupling blockades in SDs in different regions. (a3) The light evolves in real space, where $L_1 = 36.3$ is the propagation length in the first region. The plot on the right shows the average intensity distribution in the straight waveguide region. (b) Same layout as (a), but in a topologically nontrivial lattice showing the morphing of bulk modes into a zero-energy topological mode under an eigenvalue difference $\Delta\beta_1' = \Delta\beta_1$, $\Delta\beta_2' = 3\Delta\beta_1$ and the wiggling frequency $\Omega_1' = \Omega_1$, $\Omega_2' = 3\Omega_1$. The propagation length $L_1' = 38.3$ and $L_2' = 4.22$ in the first and second regions in (b3), respectively.

in Fig. 4(a3). Next, in order to couple light into a topological mode, we need to adjust the wiggling frequency, as illustrated in the following example. We excite the mode in the top band of the nontrivial ANN-designed SSH lattice, with the largest eigenvalue, and wiggle the lattice at the frequency that enables discrete transport in the upper band in SD [Fig. 4(b2)]. When the mode adjacent to the gap becomes sufficiently populated, we switch the wiggling frequency to half of the gap width ($\Omega_2' = \Delta\beta_2'$), which enables light to couple into the topological mode [Fig. 4(b2)]. After that, we turn off the wiggling, and light remains propagating in this mode. In Fig. 4(b3), we plot the corresponding dynamics in real space, which can be interpreted as morphing of light from a bulk mode into a topological edge mode merely via properly tailored control of the system (wiggling frequency).

4 Discussion and Conclusion

In summary, the new findings of this paper are mainly twofold. First, we have presented a new scheme based on ANNs for tailoring SDs by means of deep-learning neural networks. Our scheme involves designing a real-space lattice with predetermined mode eigenvalue spectra, enabling controlled coupling through time-dependent perturbations. Then, to benchmark the scheme, we have implemented it to demonstrate uniform synthetic mode coupling. Second, we have shown the potential of our approach by morphing light into a topologically protected edge mode. We envision that this ANN method will be useful in designing SDs in 2D and 3D real-space lattices, although the inverse problem of calculating the Hamiltonian from the spectrum is a challenging task in higher dimensional systems. More specifically, mode arrays designed by ANNs allow for flexible mode control and the possibility of constructing third-order topological insulators (an achievement not possible with equally spaced mode arrays[50]). We believe that the ANN approach could also be developed to design the mode structure (and therefore the matrix elements of the couplings in synthetic space) in addition to the eigenvalue structure. The potential of this work extends beyond photonics, with the possibility of uncovering geometrically inaccessible physics within various parametric spaces.[19,44] From an application standpoint, the implications are broad, including mode manipulation for enhanced mode lasing, optical switching, quantum optics, and mode-division-multiplexing data transmission.[27,28,51–55] Given that our technique primarily involves tuning the distance between waveguides and the frequency of waveguide wiggling, it holds promise for

optimal design and fabrication of integrated photonic devices. The synergy between ANN-empowered topological and SD photonics may offer a promising avenue for future photonic material and device applications.[36–38,56]

Code and Data Availability

The data and code supporting this study are available from the corresponding authors upon reasonable request.

Acknowledgments

This work was supported by the National Key R&D Program of China (Grant No. 2022YFA1404800), the National Natural Science Foundation of China (Grant Nos. 12134006, 12274242, 11922408, and 12204252), the China Postdoctoral Science Foundation (Grant Nos. BX2021134 and 2021M701790), the Natural Science Foundation of Tianjin for Distinguished Young Scholars (Grant No. 21JCJQJC00050), PCSIRT (Grant No. IRT_13R29), and the 111 Project (Grant No. B23045) in China. We acknowledge support from the Croatian-Chinese bilateral project funded by the Ministry of Science and Education in Croatia and the Ministry of Science and Technology in China. HB acknowledges support from the project "Implementation of cutting-edge research and its application as part of the Scientific Center of Excellence for Quantum and Complex Systems, and Representations of Lie Algebras," European Union, European Regional Development Fund. RM acknowledges support from the Canada Research Chair program and from NSERC via the Discovery Grant program.

References

1. T. Ozawa and H. M. Price, "Topological quantum matter in synthetic dimensions," *Nat. Rev. Phys.* **6**(5), 349–357 (2019).
2. E. Lustig and M. Segev, "Topological photonics in synthetic dimensions," *Adv. Opt. Photonics* **13**(2), 426–461 (2021).
3. O. Boada et al., "Quantum simulation of an extra dimension," *Phys. Rev. Lett.* **108**(13), 133001 (2012).
4. A. Celi et al., "Synthetic gauge fields in synthetic dimensions," *Phys. Rev. Lett.* **112**(4), 043001 (2014).
5. T. Ozawa et al., "Synthetic dimensions in integrated photonics: from optical isolation to four-dimensional quantum Hall physics," *Phys. Rev. A* **93**(4), 043827 (2016).
6. B. Lian and S.-C. Zhang, "Weyl semimetal and topological phase transition in five dimensions," *Phys. Rev. B* **95**(23), 235106 (2017).
7. S.-C. Zhang and J. Hu, "A four-dimensional generalization of the quantum Hall effect," *Science* **294**(5543), 823–828 (2001).
8. D. Jukić and H. Buljan, "Four-dimensional photonic lattices and discrete tesseract solitons," *Phys. Rev. A* **87**(1), 013814 (2013).
9. K. Wang et al., "Generating arbitrary topological windings of a non-Hermitian band," *Science* **371**(6535), 1240–1245 (2021).
10. K. Wang et al., "Topological complex-energy braiding of non-Hermitian bands," *Nature* **598**(7879), 59–64 (2021).
11. S. Weidemann et al., "Topological funneling of light," *Science* **368**(6488), 311–314 (2020).
12. A. Regensburger et al., "Parity–time synthetic photonic lattices," *Nature* **488**(7410), 167–171 (2012).
13. A. L. M. Muniz et al., "2D Solitons in PT-symmetric photonic lattices," *Phys. Rev. Lett.* **123**(25), 253903 (2019).
14. S. Weidemann et al., "Topological triple phase transition in non-Hermitian Floquet quasicrystals," *Nature* **601**(7893), 354–359 (2022).
15. C. Leefmans et al., "Topological dissipation in a time-multiplexed photonic resonator network," *Nat. Phys.* **18**(4), 442–449 (2022).
16. A. Dutt et al., "A single photonic cavity with two independent physical synthetic dimensions," *Science* **367**(6473), 59–64 (2020).
17. A. Dutt et al., "Experimental band structure spectroscopy along a synthetic dimension," *Nat. Commun.* **10**(1), 3122 (2019).
18. G. Li et al., "Direct extraction of topological Zak phase with the synthetic dimension," *Light Sci. Appl.* **12**(1), 81 (2023).
19. E. Lustig et al., "Photonic topological insulator induced by a dislocation in three dimensions," *Nature* **609**(7929), 931–935 (2022).
20. E. Lustig et al., "Photonic topological insulator in synthetic dimensions," *Nature* **567**(7748), 356–360 (2019).
21. M. Yang et al., "Topological band structure via twisted photons in a degenerate cavity," *Nat. Commun.* **13**(1), 2040 (2022).
22. M. Yang et al., "Realization of exceptional points along a synthetic orbital angular momentum dimension," *Sci. Adv.* **9**(4), eabp8943 (2023).
23. L. Yuan et al., "Synthetic dimension in photonics," *Optica* **5**(11), 1396–1405 (2018).
24. Z. Yang et al., "Mode-locked topological insulator laser utilizing synthetic dimensions," *Phys. Rev. X* **10**(1), 011059 (2020).
25. H. Buljan, D. Jukić, and Z. Chen, "Loss leads the way to utopia," *Nat. Phys.* **18**(4), 371–372 (2022).
26. N. K. Efremidis and D. N. Christodoulides, "Revivals in engineered waveguide arrays," *Opt. Commun.* **246**(4), 345–356 (2005).
27. C. Li, D. Liu, and D. Dai, "Multimode silicon photonics," *Nanophotonics* **8**(2), 227–247 (2019).
28. C. Li et al., "Subwavelength silicon photonics for on-chip mode-manipulation," *PhotoniX* **2**(1), 11 (2021).
29. M. P. Hokmabadi et al., "Supersymmetric laser arrays," *Science* **363**(6427), 623–626 (2019).
30. F. O. Wu, A. U. Hassan, and D. N. Christodoulides, "Thermodynamic theory of highly multimoded nonlinear optical systems," *Nat. Photonics* **13**(11), 776–782 (2019).
31. H. Pourbeyram et al., "Direct observations of thermalization to a Rayleigh–Jeans distribution in multimode optical fibres," *Nat. Phys.* **18**(6), 685–690 (2022).
32. W. P. Su, J. R. Schrieffer, and A. J. Heeger, "Solitons in polyacetylene," *Phys. Rev. Lett.* **42**(25), 1698–1701 (1979).
33. J. Yim et al., "Broadband continuous supersymmetric transformation: a new paradigm for transformation optics," *eLight* **2**(1), 16 (2022).
34. Y. LeCun, Y. Bengio, and G. Hinton, "Deep learning," *Nature* **521**(7553), 436–444 (2015).
35. G. Carleo et al., "Machine learning and the physical sciences," *Rev. Mod. Phys.* **91**(4), 045002 (2019).
36. G. Wetzstein et al., "Inference in artificial intelligence with deep optics and photonics," *Nature* **588**(7836), 39–47 (2020).
37. Z. Chen and M. Segev, "Highlighting photonics: looking into the next decade," *eLight* **6**(1), 2 (2021).
38. W. Ma et al., "Deep learning for the design of photonic structures," *Nat. Photonics* **15**(2), 77–90 (2021).
39. P. R. Wiecha et al., "Deep learning in nano-photonics: inverse design and beyond," *Photonics Res.* **9**(5), B182–B200 (2021).
40. Y. Shen et al., "Deep learning with coherent nanophotonic circuits," *Nat. Photonics* **11**(7), 441–446 (2017).
41. S. Pai et al., "Experimentally realized *in situ* backpropagation for deep learning in photonic neural networks," *Science* **380**(6643), 398–404 (2023).
42. L. M. Narducci and M. Orszag, "Eigenvalues and eigenvectors of angular momentum operator J_x without the theory of rotations," *Am. J. Phys.* **40**(12), 1811–1814 (1972).
43. Y. E. Kraus et al., "Topological states and adiabatic pumping in quasicrystals," *Phys. Rev. Lett.* **109**(10), 106402 (2012).
44. O. Zilberberg et al., "Photonic topological boundary pumping as a probe of 4D quantum Hall physics," *Nature* **553**(7686), 59–62 (2018)
45. S. Xia et al., "Nontrivial coupling of light into a defect: the interplay of nonlinearity and topology," *Light Sci. Appl.* **9**(1), 147 (2020).

46. T. Kreis, "Digital holographic interference-phase measurement using the Fourier-transform method," *J. Opt. Soc. Am. A* **3**(6), 847–855 (1986).
47. N. Malkova et al., "Observation of optical Shockley-like surface states in photonic superlattices," *Opt. Lett.* **34**(11), 1633–1635 (2009).
48. S. Xia et al., "Nonlinear tuning of PT symmetry and non-Hermitian topological states," *Science* **372**(6537), 72–76 (2021).
49. J. Wang et al., "Topologically tuned terahertz confinement in a nonlinear photonic chip," *Light Sci. Appl.* **11**(1), 152 (2022).
50. A. Dutt et al., "Higher-order topological insulators in synthetic dimensions," *Light Sci. Appl.* **9**(1), 131 (2020).
51. Y. Xiong, R. B. Priti, and O. Liboiron-Ladouceur, "High-speed two-mode switch for mode-division multiplexing optical networks," *Optica* **4**(9), 1098–1102 (2017).
52. K. Chen et al., "Broadband optical switch for multiple spatial modes based on a silicon densely packed waveguide array," *Opt. Lett.* **44**(4), 907–910 (2019).
53. L.-T. Feng et al., "On-chip coherent conversion of photonic quantum entanglement between different degrees of freedom," *Nat. Commun.* **7**(1), 11985 (2016).
54. A. Mohanty et al., "Quantum interference between transverse spatial waveguide modes," *Nat. Commun.* **8**(1), 14010 (2017).
55. H. Jia et al., "WDM-compatible multimode optical switching system-on-chip," *Nanophotonics* **8**(5), 889–898 (2019).
56. A. Balčytis et al., "Synthetic dimension band structures on a Si CMOS photonic platform," *Sci. Adv.* **8**(4), eabk0468 (2022).

Shiqi Xia is a professor in the TEDA Institute of Applied Physics and School of Physics in Nankai University. He received his PhD from Nankai University in 2021. His research interests include topological photonics, non-Hermitian optics, and synthetic dimensions.

Sihong Lei is a PhD student working under supervision of Prof. Daohong Song and Prof. Zhigang Chen in the TEDA Institute of Applied Physics and School of Physics at Nankai University. She is currently working on pseudospin and topological phase mapping.

Roberto Morandotti received his MSc degree in physics from the University of Genova, Genova, Italy, in 1993 and his PhD from the University of Glasgow, Glasgow, United Kingdom, in 1999. Since 2003, he is with INRS-EMT, Varennes, Canada. His current research interests include integrated and quantum optics, as well as terahertz science and applications. He is a Fellow of the Royal Society of Canada, AAAS, IEEE, APS, Optica, and SPIE, and an E.W.R Steacie Memorial Fellow (2011), a recipient of the NSERC Synergy (2019) and Brockhouse Awards (2020), as well as of the Prix Marie-Victorin (2022) and the Prix Urgel-Archambault (2023).

Hrvoje Buljan is a full professor at the University of Zagreb with more than 90 publications and 6000 citations in Google Scholar. His expertise is in photonics and condensed-matter physics. He received the Croatian State Award for Science in 2010, the Andrija Mohorovii award in 2019, and the Croatian Academy of Sciences award in 2023. He is the PI for the Scientific Center of Excellence for Quantum and Complex Systems (80 scientists, 9 institutions, and 5 MEUR EU-funding).

Zhigang Chen earned his PhD from Bryn Mawr College and was a research staff member at Princeton University before joining the faculty at San Francisco State University where he became a full professor in 2006. He is currently a chair professor at Nankai University. His research interests include nonlinear optics, topological photonics, and optical manipulation. He has served as an editor for several journals and as a chair for numerous conferences, including General Co-Chair for CLEO-Fundamental Science. He is a fellow of OSA and APS.

Biographies of the other authors are not available.